

ADAPTIVE RESOLUTION OF MAINLOBE AND SIDELOBE DETECTIONS USING MODEL ORDER DETERMINATION

Amin G. Jaffer, Joe C. Chen, and Thomas W. Miller

Raytheon Electronic Systems
2200 E. Imperial Highway
Los Angeles, California 90009-2426
e-mail: ajaffer@west.raytheon.com

ABSTRACT

This paper presents the development and performance evaluation of a methodology for distinguishing between mainlobe and sidelobe detections that arise in adaptive radar systems operating in adverse environments. Various adaptive detection test statistics such as the adaptive matched filter (AMF), the generalized likelihood ratio test (GLRT) and adaptive coherence estimate (ACE), and combinations of these, have been previously analyzed with respect to their sidelobe rejection capabilities. In contrast to these methods which are based on detecting a single target with known direction and Doppler, the present method uses model order determination techniques applied to the AMF or GLRT data observed over the range of unknown angle and Doppler parameters. The determination of model order, i.e., the number of signals present in the data, is made by using least-squares model fit error residuals and applying the Akaike Information Criterion. Comprehensive computer simulation results are presented which demonstrate substantial improvement in sidelobe rejection performance compared to previous methods.

1. INTRODUCTION

A variety of constant false-alarm rate (CFAR) adaptive detection statistics have been developed and analyzed for radar target detection in adverse environments [1]-[8]. Adaptive beamforming, adaptive filtering and, generally, joint space-time adaptive processing (STAP) methods are being increasingly considered for airborne radar detection of low-Doppler targets immersed in ground clutter and subject to directional noise jamming. An important issue that needs to be considered is the sidelobe performance of these adaptive detection algorithms. “False” sidelobe detections can arise due to undernulled interferences, intrinsically high sidelobes generated by the adaptive beamforming space-time algorithms used with limited data snapshots, and other reasons. This can result in an unacceptably high false alarm rate. Previous works have focused on determining the sidelobe rejection performance of the adaptive matched filter (AMF) test [3],[6], the generalized likelihood ratio test (GLRT) of Kelly [1], the adaptive coherence estimator (ACE) test and a cascade of AMF/ACE test [4] or AMF/GLRT test [8]. It is to be noted that all of these previous methods are based on applying adaptive detection criteria developed for detecting a single target signal with known direction and Doppler in correlated noise. In contrast to this, the present work uses multiple maximum-likelihood model order fits to the AMF or GLRT data

observed over the range of the unknown angle and Doppler parameters. The resulting fit error residuals are used in the Akaike Information Criterion (AIC) to deduce the correct model order and thereby reject “false” sidelobe detections.

2. MAXIMUM-LIKELIHOOD MODEL ORDER DETERMINATION USING AMF OR GLRT

We begin by considering two well-known adaptive detection methods, AMF and GLRT, as a starting point for our new method described below and also for performance comparison purposes. We consider an N -element array and seek to determine the presence of one or more signals in an observation vector (or snapshot) \mathbf{x} called the test cell. The methodology developed here applies to the general STAP problem where the data vector \mathbf{x} can be a concatenated space-time vector of array element data and coherent pulse samples; however, the computer simulation results presented in section 3 use only simulated spatial array data so our development here will be mainly presented in that context.

Consider then that the AMF [3] and GLRT [1] metrics have been computed as a function of angle (azimuth) and result in the following test:

$$J_{\text{AMF}}(\theta) = \frac{|\mathbf{d}(\theta)^H \hat{\mathbf{R}}^{-1} \mathbf{x}|^2}{\mathbf{d}(\theta)^H \hat{\mathbf{R}}^{-1} \mathbf{d}(\theta)} = \left| \mathbf{w}(\theta)^H \mathbf{x} \right|^2 \stackrel{H_1}{\geq} \stackrel{H_0}{\leq} K\alpha_{\text{AMF}}, \quad (1)$$

where $\mathbf{d}(\theta)$ is the signal steering vector for angle θ , i.e., the array response vector, $\hat{\mathbf{R}}$ is the sample covariance matrix of the interference plus noise (whose true covariance matrix is \mathbf{R}), based on an auxiliary set of K data vectors \mathbf{x}_i , $i = 1, \dots, K$ which share the same interference plus noise only covariance matrix with the test data \mathbf{x}

$$\hat{\mathbf{R}} = \frac{1}{K} \sum_{i=1}^K \mathbf{x}_i \mathbf{x}_i^H, \quad (2)$$

and $K\alpha_{\text{AMF}}$ is the threshold which can be determined numerically for a given false alarm P_{FA} . The hypothesis H_1 denotes signal plus noise and the null hypothesis H_0 denotes noise only. An alternate form is shown on the right side of (1) where an array weight vector $\mathbf{w}(\theta)$ can be defined as $\mathbf{w}(\theta) = \hat{\mathbf{R}}^{-1} \mathbf{d}(\theta) / \sqrt{\mathbf{d}(\theta)^H \hat{\mathbf{R}}^{-1} \mathbf{d}(\theta)}$. Equation (1) represents the adapted array output for the test vector \mathbf{x} normalized by the output interference plus noise power.

In order to control the sidelobe response of the adaptive array, the weight vector $\mathbf{w}(\theta)$ is often computed as $\mathbf{w}(\theta) = \widehat{\mathbf{R}}^{-1} \mathbf{d}_{sh}(\theta) / \sqrt{\mathbf{d}_{sh}(\theta)^H \widehat{\mathbf{R}}^{-1} \mathbf{d}_{sh}(\theta)}$, where $\mathbf{d}_{sh}(\theta) = \mathbf{d}(\theta) \odot \mathbf{w}_T$ and \mathbf{w}_T is an appropriate taper or shading function, and \odot denotes the element-by-element Schur product.

The GLRT test is

$$J_{\text{GLRT}}(\theta) = \frac{J_{\text{AMF}}(\theta)}{1 + \frac{1}{K} \mathbf{x}^H \widehat{\mathbf{R}}^{-1} \mathbf{x}} \stackrel{H_0}{\gtrless} K\gamma, \quad (3)$$

where $K\gamma$ is the threshold which can be determined for a given false alarm P_{FA} . The $J_{\text{AMF}}(\theta)$ or $J_{\text{GLRT}}(\theta)$ are evaluated at some discrete set of points in the angle θ which covers the range of expected target angles. Note that as far as variation with θ is concerned, $J_{\text{GLRT}}(\theta)$ is merely proportional to $J_{\text{AMF}}(\theta)$ since the denominator in (3) does not depend explicitly on the search variable θ . An example of the $J_{\text{AMF}}(\theta)$ function for a single target is shown in Figure 1. Note that if all peaks above the threshold, which has been set for a probability of false alarm P_{FA} of 10^{-6} , were to be considered detections the figure shows that there should be six detections of which five of them would be false alarms (solid line). Even if a Chebyshev taper with -50dB sidelobe level is used, there are still two false detections (dashed line). The shading is only partly effective in the presence of interferences, in this case one jammer at -30 degrees.

Now assume that the test data vector contains m target signals, $m = 0, 1, \dots, M$ where the maximum number M may be known from system considerations. Then,

$$\mathbf{x} = \mathbf{D}_s \mathbf{a} + \mathbf{n}, \quad (4)$$

where $\mathbf{D}_s = [\mathbf{d}(\theta_{s1}), \dots, \mathbf{d}(\theta_{sm})]$ is a $N \times m$ matrix of target steering vectors and \mathbf{a} is an $m \times 1$ vector of complex amplitudes of the m signals. The complex value of the $J_{\text{AMF}}(\theta)$ function represents the application of the weight vector $\mathbf{w}(\theta)$ to the vector \mathbf{x} resulting in the expression

$$y(\theta) = \mathbf{w}(\theta)^H \mathbf{x} = \mathbf{w}(\theta)^H \mathbf{D}_s \mathbf{a} + v(\theta), \quad (5)$$

where $v(\theta) = \mathbf{w}(\theta)^H \mathbf{n}$. We assume that $y(\theta)$ has been evaluated at K_P distinct points $\theta_1, \dots, \theta_{K_P}$, where $m \leq K_P \leq N$. These points would include the peaks of the $J_{\text{AMF}}(\theta)$ function. We have

$$\begin{bmatrix} y_1 \\ \vdots \\ y_{K_P} \end{bmatrix} = \begin{bmatrix} \mathbf{w}(\theta_1)^H \mathbf{D}_s \mathbf{a} \\ \vdots \\ \mathbf{w}(\theta_{K_P})^H \mathbf{D}_s \mathbf{a} \end{bmatrix} + \begin{bmatrix} v(\theta_1) \\ \vdots \\ v(\theta_{K_P}) \end{bmatrix}, \quad (6)$$

or, compactly,

$$\mathbf{Y} = \mathbf{H} \mathbf{a} + \mathbf{v}, \quad (7)$$

where $\mathbf{H} = \mathbf{W}^H \mathbf{D}_s$ and $\mathbf{W} = [\mathbf{w}(\theta_1), \dots, \mathbf{w}(\theta_{K_P})]$, and $\mathbf{v} = [v(\theta_1), \dots, v(\theta_{K_P})]^T$. The covariance matrix of \mathbf{v} is

$$\mathbf{R}_v = E[\mathbf{v} \mathbf{v}^H] = \mathbf{W}^H \mathbf{R} \mathbf{W}. \quad (8)$$

Under the assumption of Gaussian statistics for the interference plus noise vector \mathbf{n} , the maximum-likelihood estimates of the amplitude vector \mathbf{a} and the angles $\Theta_s = [\theta_{s1}, \dots, \theta_{sm}]$ are obtained by minimizing the nonlinear weighted least-squares criterion

$$\begin{aligned} J_{\text{ML}}(\mathbf{a}, \Theta_s) &= [\mathbf{Y} - \mathbf{H} \mathbf{a}]^H \mathbf{R}_v^{-1} [\mathbf{Y} - \mathbf{H} \mathbf{a}] \\ &= \left\| \mathbf{R}_v^{-1/2} [\mathbf{Y} - \mathbf{H} \mathbf{a}] \right\|^2, \end{aligned} \quad (9)$$

where $\mathbf{R}_v^{-1/2}$ is the square-root of the Hermitian positive-definite matrix \mathbf{R}_v^{-1} and $\|\cdot\|$ denotes the Euclidean norm of a vector. Let $\mathbf{Z} = \mathbf{R}_v^{-1/2} \mathbf{Y}$, the “whitened” data vector and $\mathbf{H}_w = \mathbf{R}_v^{-1/2} \mathbf{H}$. Then,

$$J_{\text{ML}}(\mathbf{a}, \Theta_s) = \|\mathbf{Z} - \mathbf{H}_w(\Theta_s) \mathbf{a}\|^2. \quad (10)$$

For a given Θ_s , J_{ML} is minimized with respect to \mathbf{a} when

$$\hat{\mathbf{a}} = \left[\mathbf{H}_w^H(\Theta_s) \mathbf{H}_w(\Theta_s) \right]^{-1} \mathbf{H}_w^H(\Theta_s) \mathbf{Z}. \quad (11)$$

Substitution of $\hat{\mathbf{a}}$ as given by (11) into (10) yields the weighted least-squares residual J_{ML} as

$$J_{\text{ML}}(\hat{\mathbf{a}}, \Theta_s) = \|(\mathbf{I} - \mathbf{P}(\Theta_s)) \mathbf{Z}\|^2, \quad (12)$$

where $\mathbf{P}(\Theta_s) \equiv \mathbf{H}_w(\Theta_s) [\mathbf{H}_w^H(\Theta_s) \mathbf{H}_w(\Theta_s)]^{-1} \mathbf{H}_w^H(\Theta_s)$ is the orthogonal projection operator and \mathbf{I} is the identity matrix. Equation (12) can be further minimized with respect to Θ_s yielding the maximum-likelihood estimate $\hat{\Theta}_s$. However, it is noted that this is a nonlinear optimization problem which may be computationally expensive to solve for $m \geq 2$. For the class of sidelobe detection problems considered here, the targets are likely to be separated from each other by more than a beamwidth and the locations of the peaks of the $J_{\text{AMF}}(\theta)$ function (which can be readily computed) provide reasonably accurate estimate of Θ_s and are used to evaluate (12).

The number of target signals is determined by applying the procedure described above for model orders $m = 1, 2, \dots, M$ and choosing that m for which the Akaike Information Criterion [9],[10] given below is a minimum:

$$\begin{aligned} AIC(m) &= -\log(\text{Likelihood function}|\hat{\mathbf{a}}, \hat{\Theta}_s, m) \\ &+ (\text{number of independently} \\ &\text{adjusted parameters in model}) \\ &= J_{\text{ML}}(\hat{\mathbf{a}}, \hat{\Theta}_s) + 3m, \end{aligned} \quad (13)$$

where $J_{\text{ML}}(\hat{\mathbf{a}}, \hat{\Theta}_s)$ is given by (12) and the approximate estimate $\hat{\Theta}_s$ discussed above is used. The method derived here is referred to as the Multi-Target AMF (MT-AMF) method.

3. PERFORMANCE EVALUATION

The P_{FA} of the GLRT test is given by [3]

$$P_{\text{FA,GLRT}} = \frac{1}{(1 + \alpha)^L}, \quad (14)$$

where $L \equiv K + 1 - N$, $\alpha = \gamma / (1 + \gamma)$, and γ is the threshold term of (3). The threshold for the AMF is determined by evaluating the following integral using numerical integration and bisection iterations as in [3]:

$$P_{\text{FA,AMF}} = \int_0^1 \frac{f_\beta(\rho; L + 1, N - 1)}{(1 + \rho \alpha_{\text{AMF}})^L} d\rho, \quad (15)$$

where

$$f_\beta(x; n, m) = \frac{(n + m - 1)!}{(n - 1)!(m - 1)!} x^{n-1} (1 - x)^{m-1} \quad (16)$$

is the central Beta density function, and ρ is the loss factor which considers the SNR loss due to finite number of snapshots in the sample covariance matrix. The analytic form of the probability of detection for a single source is also given in [3] which we excluded for brevity. Our Monte Carlo simulation results have been confirmed to match these analytical curves.

We consider a linear equally spaced array of 10 elements with half-wavelength spacing (nominal beamwidth = 12 degrees) for all the simulations provided in this section. A noise jammer signal of strength 40dB relative to thermal noise is placed at -30 degrees and the P_{FA} is set to be 10^{-6} . The scanning angles are from -50 to 50 degrees in azimuth. A single source of varying SNR is placed at broadside and the performance of the algorithms in single source detection and false sidelobe rejections are compared. The AMF detection only relies on the peaks above the given threshold, but the MT-AMF test takes the peaks and tests for model order $m = 1$ and 2 . If $m = 1$ is decided, the overall peak is retained as an indicator of a single signal and the other peaks are rejected. The probability of detecting the mainlobe signal is plotted in Figure 2, regardless of the number of peaks or model decisions, after 5000 Monte Carlo runs. We observe no loss in the detection for the MT-AMF method. Then, the probability of false sidelobe detections is plotted for the two algorithms in Figure 3. The AMF gives rise to high false sidelobe detections at high SNR, but the MT-AMF greatly reduces the false sidelobe detections and its probability also saturates as SNR increases. The false sidelobe detections of the proposed method go down rapidly for increasing K and the lower bound is for $K = \infty$, which is the multi-target matched filter. For tapered weight vector $\mathbf{w}(\theta)$, we also compare the sidelobe rejections performance, as depicted in Figure 4. Note that the use of a taper with the conventional AMF method only reduces sidelobe detections slightly at the cost of a slight decrease in mainlobe detection probability (not shown). However, the use of model order determination using AIC with tapered AMF data shows almost the same dramatic improvement in reducing false sidelobe detections as before with the same mainlobe detection probability as the conventional tapered AMF.

Then, two sources of equal strength are placed at broadside and 45 degrees. The probability of detecting both sources within a ± 10 degrees angle constraint is plotted for the AMF and MT-AMF algorithms, as depicted in Figure 5. We observe the same detections between the conventional method and the proposed algorithm. The two sources detections using the GLRT is plotted in Figure 6. However, for $K = 20$, the GLRT yields extremely poor performance in detecting both sources due to the normalization factor in the denominator of (3). The derivation of the GLRT is under the assumption of a single source; therefore, despite its advantage in sidelobe rejections for lower K , as depicted in Figure 7, and single source detections, it is not an appropriate model for two sources.

4. CONCLUSIONS

In this paper, we have shown substantial false sidelobe rejection improvement using the proposed model order determination method. The algorithm is efficient in computations and can be easily implemented in existing adaptive radar systems.

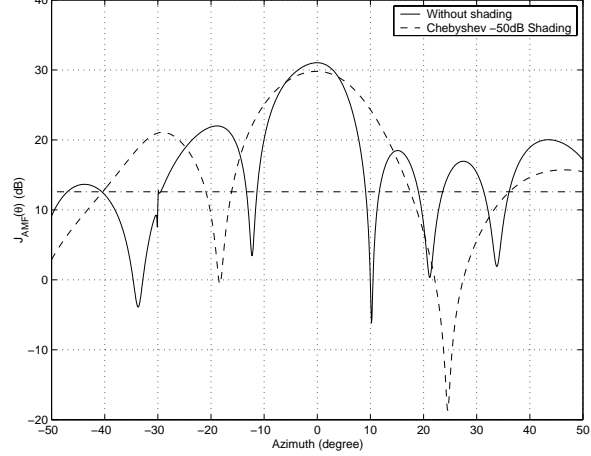


Fig. 1. $J_{AMF}(\theta)$ function for a 20dB signal at broadside, $N = 10$, $K = 100$, $PFA = 10^{-6}$.

5. REFERENCES

- [1] E.J. Kelly, "An Adaptive Detection Algorithm," *IEEE Trans. on Aerospace and Electronics Systems*, vol. AES-22, no. 1, pp. 115-127, Mar. 1986.
- [2] E.J. Kelly, "Performance of an Adaptive Detection Algorithm: Rejection of Unwanted Signals," *IEEE Trans. on Aerospace and Electronics Systems*, vol. AES-25, no. 2, pp. 122-133, Mar. 1989.
- [3] F.C. Robey, D.R. Fuhrmann, E.J. Kelly, R. Nitzberg, "A CFAR Adaptive Matched Filter Detector," *IEEE Trans. on Aerospace and Electronics Systems*, vol. 28, no. 1, pp. 208-216, Mar. 1992.
- [4] D. E. Kreithen, C.F. Pearson, C.D. Richmond, "Adaptive Sidelobe Blanker: A Novel Method of Performance Evaluation and Threshold Setting in the Presence of Inhomogeneous Clutter," in *Proc. 32nd Asilomar Conf. Signals Syst. & Comp.*, vol. 2, pp.528-32, Pacific Grove, CA, Nov. 1998.
- [5] C.D. Richmond, "Performance of the Adaptive Sidelobe Blanker Detection Algorithm in Homogeneous Environments," *IEEE Trans. on Signal Processing*, vol. 48, no. 5, pp. 1235-47, May 2000.
- [6] C.D. Richmond, "Performance of a Class of Adaptive Detection Algorithms in Nonhomogeneous Environments," *IEEE Trans. on Signal Processing*, vol. 48, no. 5, pp. 1248-62, May 2000.
- [7] R.A. Monzingo, T.W. Miller, *Introduction to Adaptive Arrays*, John Wiley, New York, 1980.
- [8] N.B. Pulsone, M.A. Zatman, "A Computational Efficient Two-Step Implementation of the GLRT," *IEEE Trans. on Signal Processing*, vol. 48, no. 3, pp 609-616, Mar. 2000.
- [9] H. Akaike, "A New Look at the Statistical Model Identification," *IEEE Trans. on Automatic Control*, vol. AC-19, pp. 716-723, Dec. 1974.
- [10] A.G. Jaffer, "Maximum-Likelihood Angular Resolution of Multiple Sources," in *Proc. 19th Asilomar Conf. Signals Syst. & Comp.*, pp.68-72, Pacific Grove, CA, Nov. 1985.

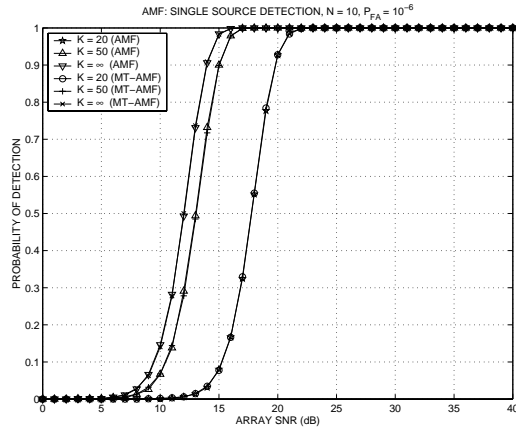


Fig. 2. Probability of detecting single mainlobe target signal using AMF and MT-AMF. Note equal performances of the two methods.

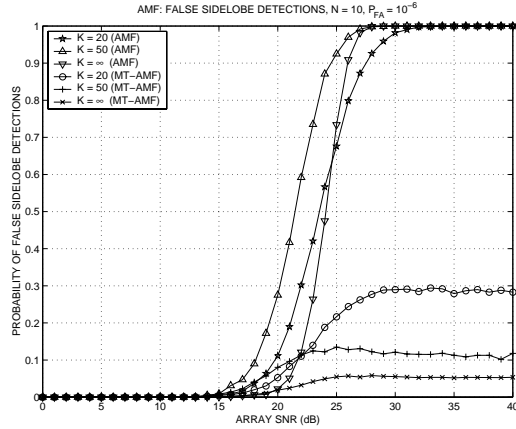


Fig. 3. Probability of false sidelobe detections using AMF and MT-AMF. Note the substantial improvement of the MT-AMF method in false sidelobe rejections at high SNR.

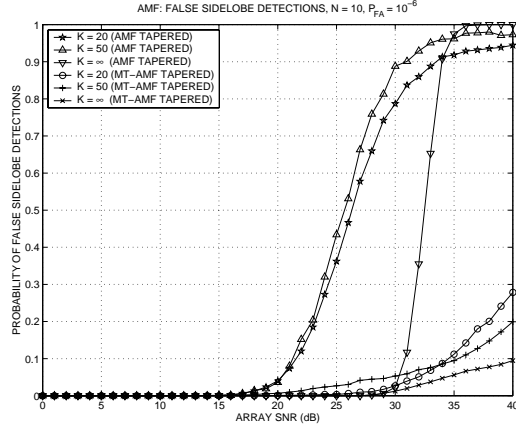


Fig. 4. Probability of false sidelobe detections using tapered AMF weights (-50dB Chebyshev). Note significant improvement even when taper is used.

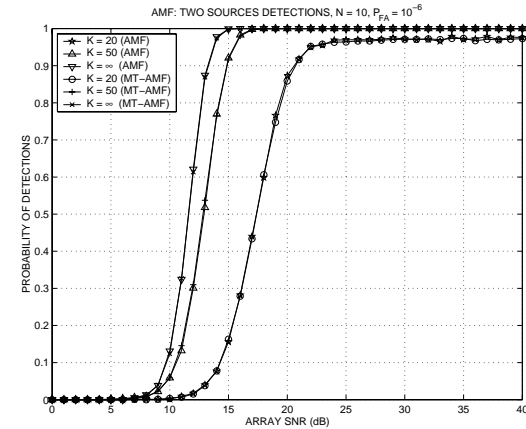


Fig. 5. Probability of detecting both sources within ± 10 degrees using AMF and MT-AMF. Note equal performances of the two.

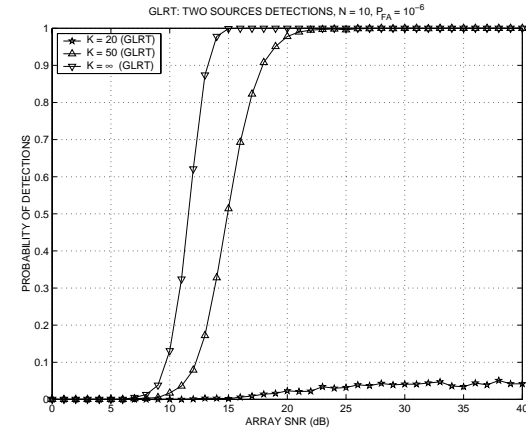


Fig. 6. Probability of detecting both sources within ± 10 degrees using GLRT. Note the degraded performance, especially for smaller K .

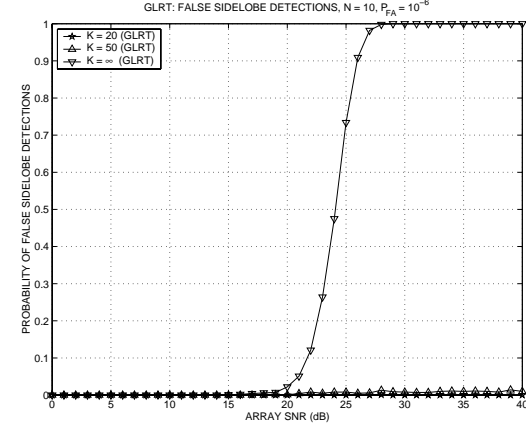


Fig. 7. Probability of false sidelobe detections using GLRT. Note good sidelobe rejection capability for smaller K at the expense of reduced detections of two sources (Fig. 6).